

## Supplementary Material

### Supplementary Note 1 – Derivation of a rational curve between surface temperature and debris thickness, from the surface energy balance equation of a debris-covered surface

The surface energy balance of a debris-covered surface (Nakawo and Young, 1981; Nicholson and Benn, 2006):

$$Q_s + Q_l + Q_h + Q_e + Q_c = 0 \quad (1)$$

where  $Q_s$  and  $Q_l$  are radiative components,  $Q_h$  and  $Q_e$  are turbulent heat flux components and  $Q_c$  is the conductive heat flux.

Surface temperature contributes to all terms except  $Q_s$  (Nicholson and Benn, 2006), thus:

$$Q_s = a \quad (2)$$

$$Q_l = b (T_s) \quad (3)$$

$$Q_h = c (T_s) \quad (4)$$

$$Q_e = d (T_s) \quad (5)$$

where  $a$ ,  $b$ ,  $c$  and  $d$  are constants.

Surface temperature and debris thickness contribute to the  $Q_c$  term. Averaged over daily timescales, debris temperatures profiles are approximately linear (Nicholson and Benn, 2006; Nicholson and Benn, 2013), so the conductive heat flux can be approximated as:

$$Q_c = \frac{k (T - T_i)}{d_t} \quad (6)$$

where  $k$  is a thermal conductivity constant,  $T$  is surface temperature (K),  $T_i$  is the temperature of melting ice (273.15K) and  $d_t$  is debris thickness.  $T - T_i =$  surface temperature ( $T_s$ ) in °C.

Thus, if equation (1) is rearranged in terms of surface temperature ( $T_s$ ) and debris thickness ( $d_t$ ):

$$a + b(T_s) + c(T_s) + d(T_s) + k \frac{T_s}{d_t} = 0 \quad (7)$$

$$a(d_t) + b(T_s)(d_t) + c(T_s)(d_t) + d(T_s)(d_t) + k(T_s) = 0 \quad (8)$$

$$a(d_t) + b(T_s)(d_t) + c(T_s)(d_t) + d(T_s)(d_t) = -k(T_s) \quad (9)$$

$$d_t (a + b(T_s) + c(T_s) + d(T_s)) = -k(T_s) \quad (10)$$

$$d_t (a + T_s(b + c + d)) = -k(T_s) \quad (11)$$

$$d_t = -k \frac{(T_s)}{a + T_s (b+c+d)} \quad (12)$$

$$d_t = \frac{(T_s)}{c_1 + c_2(T_s)} \quad \text{if } c_1 = \frac{a}{-k} \text{ and } c_2 = \frac{b+c+d}{-k} \quad (13)$$

Therefore, a rational curve form of the relationship between surface temperature and debris thickness can be derived from the surface energy balance equation for a debris-covered glacier surface.

## Supplementary Note 2 – Supplementary equations and tables for LST calculation

### Supplementary Note 2(i)

$$L_{sen} = M_l Q_{cal} + A_l \quad (14)$$

where  $L_{sen}$  is top of atmosphere radiance,  $M_l$  is the multiplicative rescaling factor ( $3.3420 \times 10^{-4}$ ),  $Q_{cal}$  is the digital number and  $A_l$  is the radiance additive rescaling factor (0.10).

### Supplementary Note 2(ii)

$$T_{sen} = \frac{c_2}{\ln(c_1/L_{sen} + 1)} \quad (15)$$

where  $T_{sen}$  is the top of atmosphere brightness temperature,  $c_1$  and  $c_2$  are thermal conversion constants (774.8853 and 1321.0789, respectively).

### Supplementary Note 2(iii)

The single-channel atmospheric correction algorithm (Jiménez-Muñoz *et al.*, 2014):

$$T_s = \gamma \left[ \frac{1}{\varepsilon_s} (\varphi_1 L_{sen} + \varphi_2) + \varphi_3 \right] + \delta \quad (16)$$

where  $\varepsilon_s$  is surface emissivity. The mean emissivity of Bands 13 and 14 of the ASTER GDEM emissivity product was used, which together have a spectral range of 10.25-11.65  $\mu\text{m}$ . This product was chosen because it is most similar to the spectral range of Landsat 8 Band 10 (10.60-11.19  $\mu\text{m}$ ) (Hulley *et al.*, 2015).  $\gamma$  and  $\delta$  in Equation 4.3 are parameters given by:

$$\gamma = \frac{T_{sen}^2}{b_\gamma L_{sen}} \quad (17)$$

$$\delta = T_{sen} - \frac{T_{sen}^2}{b_\gamma} \quad (18)$$

and  $\psi_1$ ,  $\psi_2$  and  $\psi_3$  are atmospheric parameters given by:

$$\varphi_1 = \frac{1}{\tau} \quad (19)$$

$$\varphi_2 = -L \downarrow - \frac{L \uparrow}{\tau} \quad (20)$$

$$\varphi_3 = L \downarrow \quad (21)$$

where  $b_\gamma$  is  $c_2/\lambda$  (1324),  $\tau$  is atmospheric transmissivity,  $L \downarrow$  is incoming solar radiation and  $L \uparrow$  is outgoing solar radiation. Values of  $\tau$ ,  $L \downarrow$  and  $L \uparrow$  were obtained for each of the six individual glaciers (Table 4.2) using the NASA atmospheric correction parameter calculator, which calculates the required atmospheric correction parameters from spectral response curves generated using the MODTRAN software (Barsi *et al.*, 2003, 2005).

Summary of the atmospheric correction parameters:

		Baltoro	Satopanth	Lirung	Ngozumpa	Changri Nup	Hailuogou
Input*	D/M/Y	15/07/13	15/07/13	15/07/16	15/07/16	15/07/15	15/07/13
	hr:min	05:30	05:20	04:50	04:40	04:40	03:50
	Lat (°N)	35.76	30.78	28.25	28.02	27.97	29.59
	Lon (°E)	76.41	79.32	85.54	86.70	86.80	101.93
Output	$\tau$	0.85	0.55	0.47	0.84	0.33	0.83
	$L\uparrow$	1.07	3.34	4.23	1.08	5.15	1.16
	$L\downarrow$	1.81	5.03	6.14	1.79	7.33	1.94

\*D/M/Y hr:min was taken to be the mid-point of the melt season in the year the debris thickness measurements were made, at the time at which Landsat 8 passes. The latitude and longitude was taken to be the mid-point of each glacial outline.

### Supplementary Note 2(iv)

The values of  $\tau$ ,  $L\downarrow$  and  $L\uparrow$  vary significantly over space, which proves a challenge when calculating the land surface temperature over the larger HMA region. An approximation of the atmospheric functions ( $\psi_1$ ,  $\psi_2$  and  $\psi_3$ ) in relation to the atmospheric water vapour content of the atmosphere (Muñoz *et al.*, 2014), in a second-order polynomial fit ( $x^2 + x + c$ ) is:

$$\begin{bmatrix} \varphi_1 \\ \varphi_2 \\ \varphi_3 \end{bmatrix} = \begin{bmatrix} c_{11} & c_{12} & c_{13} \\ c_{21} & c_{22} & c_{23} \\ c_{31} & c_{32} & c_{33} \end{bmatrix} \begin{bmatrix} w^2 \\ w \\ 1 \end{bmatrix} \quad (22)$$

where coefficients  $c_{ij}$  are obtained by simulations with many different atmospheric profile inputs and  $w$  is the atmospheric water content, obtained from the NCEP/NCAR Reanalysis Data (Kalnay *et al.*, 1996).

### Supplementary Note 2(v)

An emissivity-only correction:

$$T_s = \frac{T_{sen}}{1 + (\lambda (T_{sen}/p)) \ln(\epsilon_s)} \quad (23)$$

where  $\lambda$  is the wavelength of the emitted radiance (10.8  $\mu\text{m}$ ) and  $p$  is  $h(c/s)$  where  $h$  is Planck's constant ( $6.626 \times 10^{-34}$ ),  $c$  is the velocity of light ( $2.998 \times 10^8$ ) and  $s$  is the Boltzmann constant ( $1.38 \times 10^{-23}$ ).

### Supplementary Note 2(vi)

Model developed by Arnold and Rees (2009) to calculate the potential solar radiation reaching the glacier surface.

Summary of the input parameters for each model run to calculate the potential solar radiation over a glacier's surface:

	Baltoro	Satopanth	Lirung	Ngozumpa	Changri Nup	Hailuogou
DEM	ASTER GDEM	HMA DEM	HMA DEM	HMA DEM	HMA DEM	ASTER GDEM
DEM res. (m)	30	8	8	8	8	30
Latitude (°N)	35.74	30.76	28.22	28.00	27.95	29.59
Start day* (JD)	121	121	121	121	121	121
No. of days** (JD)	183	183	183	183	183	183
Temp. res. (mins)	60	60	60	60	60	60

\* Beginning of the melt season (1<sup>st</sup> May/JD=121)

\*\* End of the melt season (31<sup>st</sup> October/JD=304); 304 – 121 = 183

Standard deviation of the potential solar radiation on an average day in the melt season, over the full glacial extent and over only the debris-covered extent, for each of the six studied glaciers:

	$\sigma$ of potential solar radiation ( $W m^{-2}$ ) on an average day in the melt season (GAMDAM glacier outline; Sakai, 2019)	$\sigma$ of potential solar radiation ( $W m^{-2}$ ) on an average day in the melt season (Debris-covered extent; Scherler <i>et al.</i> , 2018)
Baltoro	4.90	2.50
Satopanth	4.34	2.20
Lirung	3.77	1.62
Ngozumpa	3.76	1.36
Changri Nup	3.48	1.63
Hailuogou	2.02	0.78

The standard deviation of total potential solar radiation received by the debris-covered surfaces on an average day during the melt season did not exceed  $2.50 W m^{-2}$ . This indicates that variation in radiation receipt due to shadowing is minimal.

### Supplementary Note 2(vii)

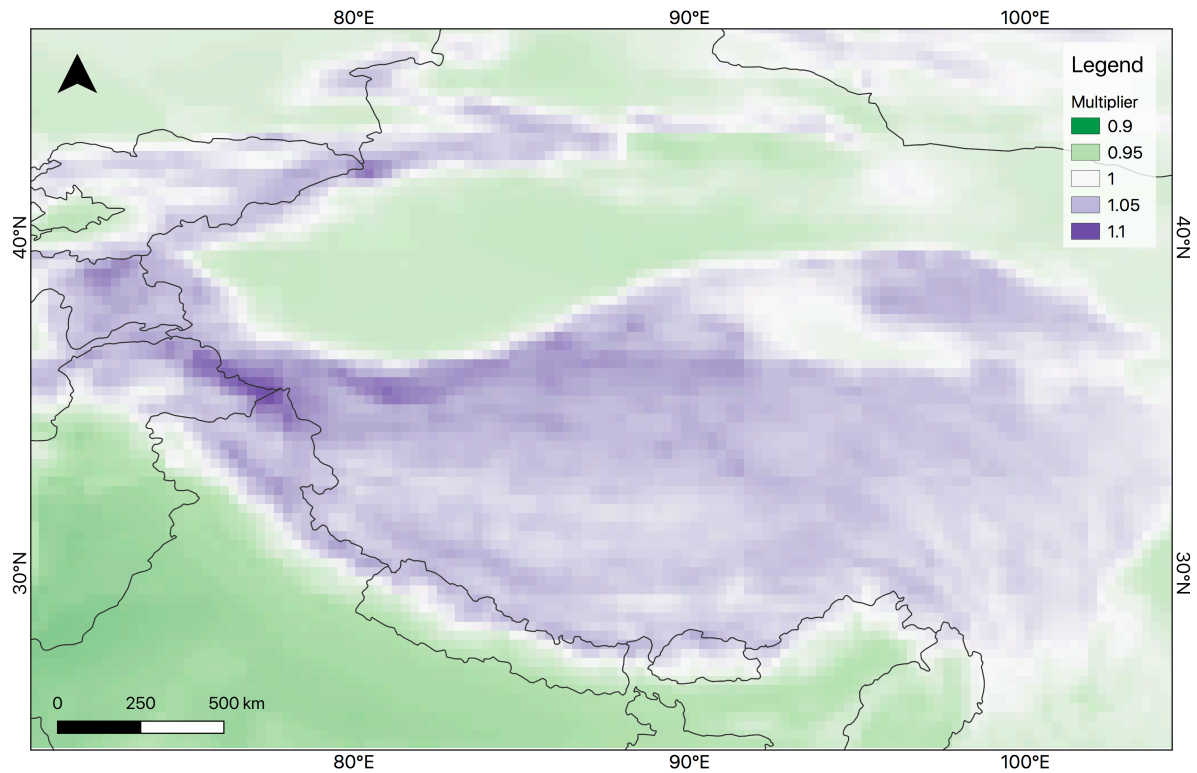
The average surface air temperature of HMA according to the ERA5 climate reanalysis data (287 K) was divided by the ERA5 climate reanalysis surface air temperature in each pixel to produce an array of multipliers with which to normalise the calculated LST composite images. If the ERA5 surface temperature  $>287 K$ , the multiplier  $<1$  and if ERA5 surface temperature  $<287 K$ , the multiplier  $>1$ .

The multipliers applied to the surface temperature for each of the studied glaciers are:

Baltoro = 1.09  
Satopanth = 1.06  
Lirung = 1.03  
Ngozumpa = 1.05  
Changri Nup = 1.05  
Hailuogou = 1.03

The multipliers applied to the surface temperature on a pixel basis to the entire HMA region are displayed in Figure S1.

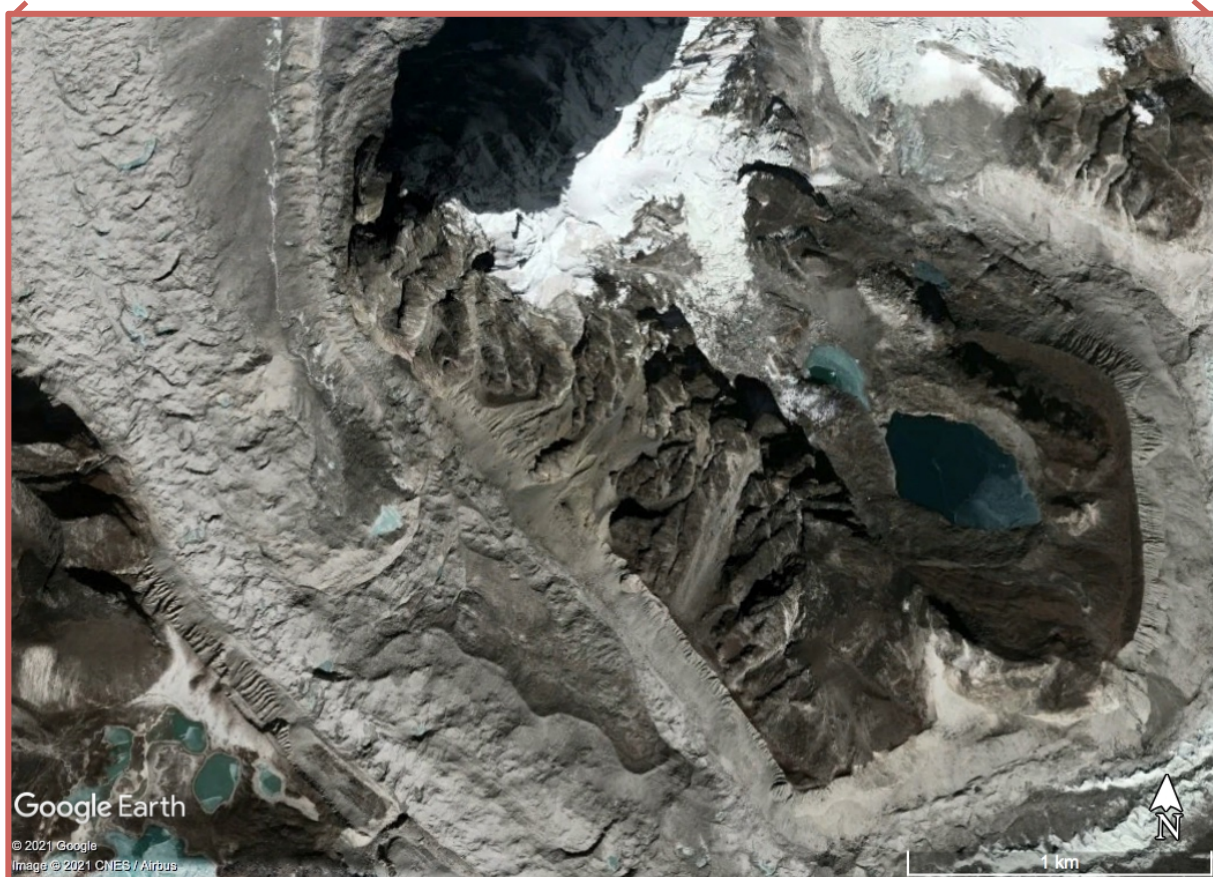
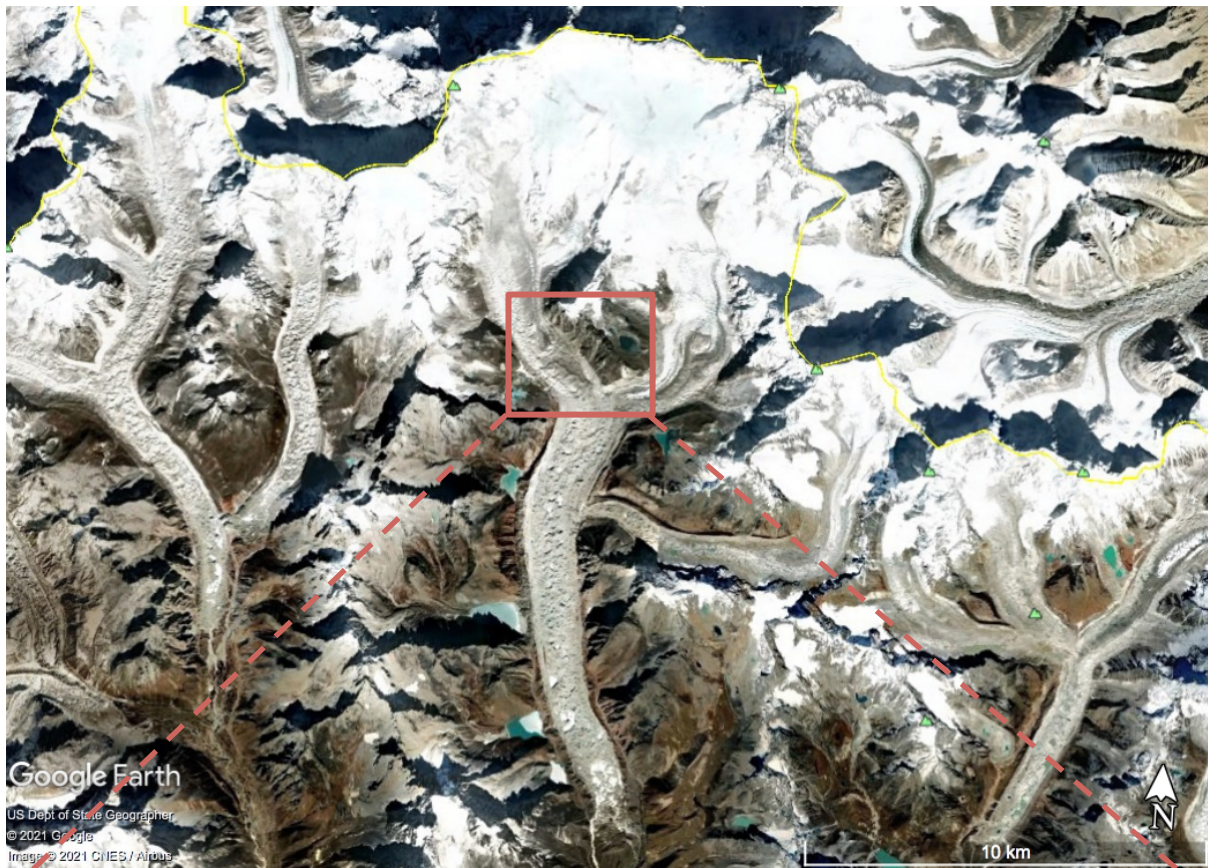
**Figure S1:** Map to show the multipliers applied to the HMA region to normalise the calculated land surface temperature.



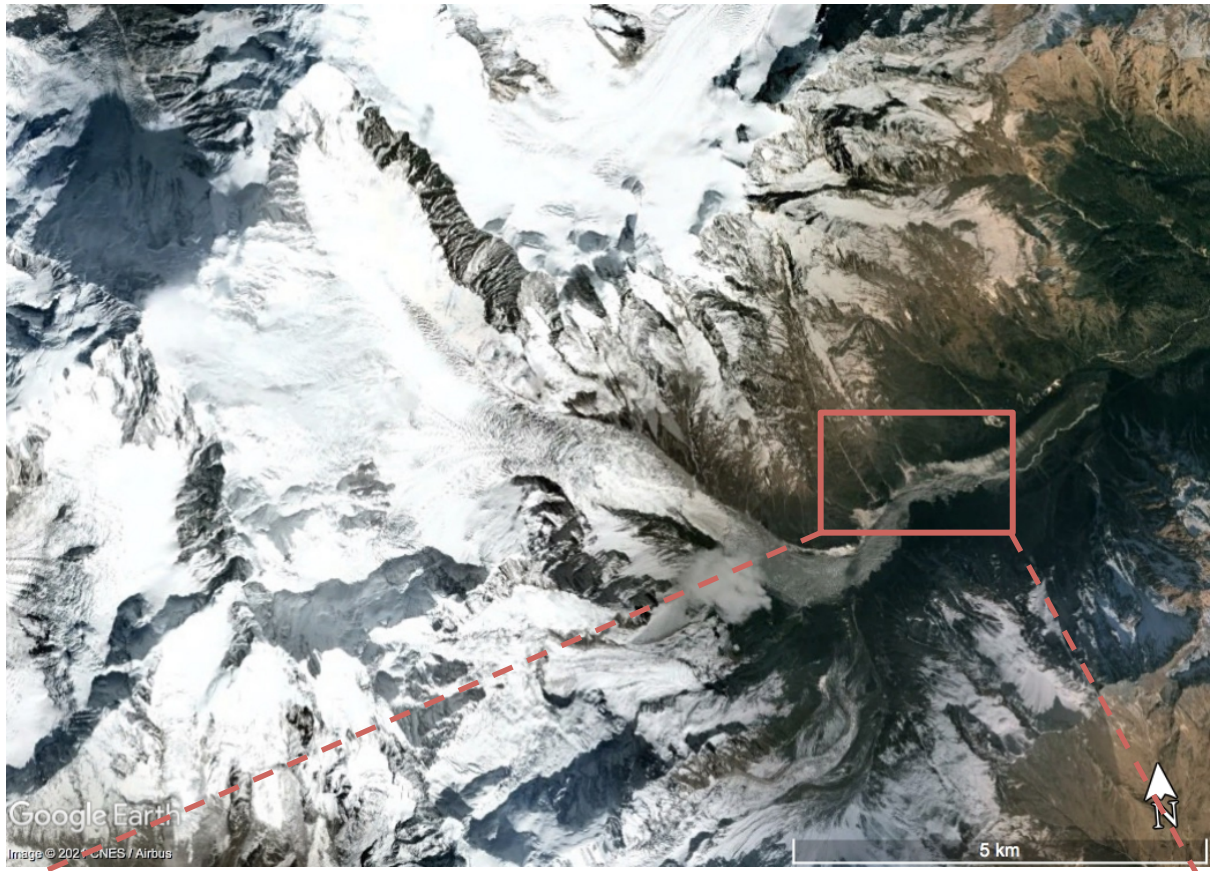
The spatial resolution of the ERA5 data is 31 km. Therefore, at the glacier scale, a single ERA5 pixel usually covered the entire extent of the glacier. The only glacier for which this was not the case was Baltoro. In this case, the ERA5 pixel covering the central point of the glacier was used. At the regional scale, normalisation was carried out based on which ERA5 pixel covered the central point of each pixel of the thermal composite image.

### Supplementary Note 3 – Simple geomorphological assessment of Google Earth imagery

Google Earth image of Ngozumpa Glacier, with a highlighted area of potential localised mass movement from the valley side



Google Earth image of Hailuoguo Glacier, with a highlighted area of potential localised mass movement from the valley side



## References

- Arnold, N.S. and Rees, W.G. (2003) Self-similarity in glacier surface characteristics. *Journal of Glaciology*, 49(167), pp.547-554. doi:10.3189/172756503781830368
- Barsi, J.A., Barker, J.L. and Schott, J.R. (2003, July) An atmospheric correction parameter calculator for a single thermal band earth-sensing instrument. In *IGARSS 2003. 2003 IEEE International Geoscience and Remote Sensing Symposium. Proceedings (IEEE Cat. No. 03CH37477)* (Vol. 5, pp. 3014-3016). IEEE. doi:10.1109/IGARSS.2003.1294665
- Barsi, J.A., Schott, J.R., Palluconi, F.D. and Hook, S.J. (2005, August) Validation of a web-based atmospheric correction tool for single thermal band instruments. In *Earth Observing Systems X* (Vol. 5882, p. 58820E). International Society for Optics and Photonics. doi:10.1117/12.619990
- Hulley, G.C., Hook, S.J., Abbott, E., Malakar, N., Islam, T. and Abrams, M. (2015) The ASTER Global Emissivity Dataset (ASTER GED): Mapping Earth's emissivity at 100 meter spatial scale. *Geophysical Research Letters*, 42(19), pp.7966-7976. doi:10.1002/2015GL065564
- Jiménez-Muñoz, J.C., Sobrino, J.A., Skoković, D., Mattar, C. and Cristóbal, J. (2014) Land surface temperature retrieval methods from Landsat-8 thermal infrared sensor data. *IEEE Geoscience and remote sensing letters*, 11(10), pp.1840-1843. doi:10.1109/LGRS.2014.2312032
- Kalnay, E., Kanamitsu, M., Kistler, R., Collins, W., Deaven, D., Gandin, L., Iredell, M., Saha, S., White, G., Woollen, J. and Zhu, Y. (1996) The NCEP/NCAR 40-year reanalysis project. *Bulletin of the American meteorological Society*, 77(3), pp.437-472. doi:10.1175/1520-0477(1996)077%3C0437:TNYRP%3E2.0.CO;2
- Nakawo, M. and Young, G.J. (1981) Field experiments to determine the effect of a debris layer on ablation of glacier ice. *Annals of Glaciology*, 2, pp.85-91. doi:10.3189/172756481794352432
- Nicholson, L. and Benn, D.I. (2006) Calculating ice melt beneath a debris layer using meteorological data. *Journal of Glaciology*, 52(178), pp.463-470. doi:10.3189/172756506781828584
- Nicholson, L. and Benn, D.I. (2013) Properties of natural supraglacial debris in relation to modelling sub-debris ice ablation. *Earth Surface Processes and Landforms*, 38(5), pp.490-501. doi:10.1002/esp.3299